

# A Quantum Computing Framework for VLBI Data Correlation

Lei Liu<sup>1</sup>

<sup>1</sup>Shanghai Astronomical Observatory, Chinese Academy of Sciences; liulei@shao.ac.cn

## Abstract

We present a quantum computing framework for VLBI data correlation. We point out that a classical baseband time series data of length  $N$  can be embedded into a quantum superposition state using amplitude encoding with only  $\log_2 N$  qubits. The basic VLBI correlation and fringe fitting operations, including fringe rotation, Fourier transform, delay compensation, and cross correlation, can be implemented via quantum algorithms with significantly reduced computational complexity. We construct a full quantum processing pipeline and validate its feasibility and accuracy through direct comparison with a classical VLBI pipeline. We recognize that amplitude encoding of large data volumes remains the primary bottleneck in quantum computing; however, the quantized nature of VLBI raw data helps reduce the state-preparation complexity. Our investigation demonstrates that quantum computation offers a promising paradigm for VLBI data correlation and is likely to play a role in future VLBI systems.

## 1 Introduction

The concept of a quantum computer was first proposed by Richard Feynman in 1981 at the First Conference on the Physics of Computation (Feynman, 1982). Inspired by Feynman’s insight, Deutsch (1985) pointed out that, by taking quantum parallelism into account, a quantum computer could solve certain computational problems faster than classical ones. Simon (1994) provided the first explicit example of an exponential quantum speed-up relative to randomized classical algorithms. Shor (1994) reformulated the integer factorization problem as period finding problem and demonstrated that the quantum Fourier transform (QFT) enables period extraction in polynomial time, therefore achieving exponential speedup compared with classical algorithms.

Since then, quantum computing developed rapidly (Michael & Chuang, 2010). In 2016, IBM released the world’s first cloud-accessible quantum computer and introduced a comprehensive software ecosystem, **Qiskit** (Javadi-Abhari et al., 2024), which supports quantum program construction, compilation and optimization through transpiler, as well as high-fidelity simulation via **Qiskit Aer**. In 2019, Google demonstrated a milestone on its 53-qubit Sycamore processor by performing a Random Circuit Sampling (RCS) task, providing the first experimental indication of the so-called “quantum supremacy” on a physical quantum device (Arute et al., 2019). In China, the Jiuzhang photonic quantum processors demonstrated quantum advantage in Gaussian Boson Sampling (GBS) task, marking the first such achievement in an photonic system (Zhong et al., 2020). The Zuchongzhi-3 105-qubit superconducting processor further extended the record of quantum computational advantage through the demonstration of enhanced random circuit sampling task (Gao et al., 2025).

The ultimate goal of quantum computing is the realization of a universal quantum computer. Although quantum computers are still in the early stages of development, scientists across multiple disciplines have begun exploring the potential applications of quantum algorithms, including quantum chemistry, combinatorial optimization, quantum machine learning (QML), finance, physical simulation, cryptanalysis, etc. (Au-Yeung et al., 2024).

Very Long Baseline Interferometry (VLBI) is the astronomical technique that achieves the highest angular resolution (Thompson et al., 2017), and has been widely used in astrophysics (Event Horizon Telescope Collaboration, 2019), astrometry (Haas et al., 2015), and orbit determination of spacecraft (Duev et al., 2012). Owing to its operation in the radio-frequency domain, VLBI relies heavily on digital signal processing, including data recording (Whitney, 2007), channelization (Zhu et al., 2016), and correlation (Zheng et al., 2010; Deller et al., 2011). It is worth mentioning that interferometric correlation requires access to

the original baseband data. Even with 1-bit or 2-bit quantization, the resulting data volume remains large. Moreover, the baseband data are actually white noise, rendering classical data compression techniques ineffective (Thompson et al., 2017). Also note that VLBI data correlation involves pairwise cross-correlation among participating stations, the total computational load scales quadratically with the number of stations. To meet the challenges posed by the rapidly growing data volumes and computational demands of next-generation facilities, dedicated data processing infrastructures are required. An example is the SKA (Dewdney et al., 2009) Regional Centre (SRC) network, which will handle the distribution, processing, and storage of 700 PB data per year<sup>1</sup>.

We point out that quantum architecture is well suited for radio interferometric data storage and processing. First of all, a system of  $n$  qubits spans a Hilbert space of dimension  $2^n$ , enabling exponentially large classical data to be represented. As a result, a classical signal of length  $N$  can be embedded into a quantum superposition state using amplitude encoding, requiring only  $\log_2 N$  qubits and achieving an impressive form of “data compression”. Moreover, linear phase manipulations, such as time-domain fringe rotation or fractional sample time correction (FSTC) in frequency-domain, can be implemented via quantum linear operators using binary decomposition, where each qubit receives a single phase rotation. This reduces the computational complexity from  $O(N)$  to  $O(\log_2 N)$ . The time to frequency domain transform can also be executed efficiently through the quantum Fourier transform (QFT), which operates with complexity  $O((\log_2 N)^2)$  (Michael & Chuang, 2010). Finally, while quantum circuits are not suitable for computing cross-power spectrum directly, the correlation between two spectrum represented as multi-qubit quantum states naturally corresponds to their inner product. Within the quantum framework, this inner product can be evaluated by constructing a unitary composite operator and extracting the result using Hadamard test (Michael & Chuang, 2010). The effect of residual delay on the cross-power spectrum can be embedded into this process, which makes post-processing fringe fitting possible. This workflow is particularly well suited for geodetic VLBI, where the extraction of delay and delay-rate observables is essential (Kondo & Takefuji, 2016).

Above analysis indicates that the construction of a quantum-based correlator is theoretically sound and technically viable. In the following sections, we provide a detailed description of the quantum operations necessary for building a quantum correlator and implement a quantum data correlation pipeline using `Qiskit`. Our work indicates that implementing a correlator using quantum circuits is not only practical but also offers substantial advantages in terms of computational complexity. This paper is organized as follows: Sec. 2 introduces the whole quantum computing framework. Sec. 3 presents the quantum pipeline and performs comparison with classical pipeline. Sec. 4 and Sec. 5 are discussion and conclusion.

## 2 The quantum computing framework

The quantum framework proposed in this work involves all the necessary quantum operations required for building the VLBI data correlation pipeline. The dataflow of the quantum pipeline is presented in Fig. 1. For comparison, the classic pipeline is also presented (Fig. 2). The detailed explanations of quantum operations are present in the following part of this section.

### 2.1 Data encoding

In classical data correlation pipeline, the voltage-sampled time series are first loaded from disk into memory and then converted from quantized bit to floating-point representations, e.g., mapping 1-bit quantization levels 0, 1 to  $-0.5, +0.5$ . In quantum framework, a system of  $n$  qubits spans a Hilbert space of dimension  $2^n$ , allowing exponentially large classical data to be represented using only a small number of qubits. In other words, a classical signal of length  $N$  after normalization can be embedded into quantum superposition state and requires only  $n = \log_2 N$  qubits:

$$\psi_x = \sum_{k=0}^{N-1} x_k |k\rangle, \quad (1)$$

---

<sup>1</sup><https://www.skao.int/en/explore/big-data/362/ska-regional-centres>

where  $x_k$  is the normalized value of the  $k$ -th sampling point:

$$\sum_{k=0}^{N-1} |x_k|^2 = 1. \quad (2)$$

If the number  $k$  is expanded in its binary representation:

$$k = \sum_{i=0}^{n-1} 2^i k_i, \quad (3)$$

then  $|k\rangle = |k_{n-1} \dots k_1 k_0\rangle$  is the  $k$ -th state of the quantum system composed of  $n$  qubits.

We use amplitude encoding to load raw data into quantum state. We have realized that this is a huge challenge to the current quantum circuits. The possible solution will be discussed in Sec. 4.1.

## 2.2 Phase modulation

For VLBI data correlation and post processing, phase modulations for the given sequence are required in several scenarios:

- Fringe rotation in the time domain:

$$x_k \rightarrow x_k e^{-j2\pi\Delta f T_s k}, \quad (4)$$

where  $\Delta f = f_0 \dot{\tau}$  is the fringe rate determined by the sky frequency  $f_0$  and delay rate  $\dot{\tau}$  given by the delay model.  $T_s = 1/f_s$  is the sampling time, which is proportional to inverse of sampling rate  $f_s$ .

- Fractional Sample Time Correction (FSTC):

$$s_k \rightarrow s_k e^{-j2\pi f_{\text{bin}} \tau_{\text{frac}} k}, \quad (5)$$

where  $f_{\text{bin}}$  is the frequency bin width in cross correlation.  $\tau_{\text{frac}}$  is the FSTC value given by the delay model.

- Fringe fitting in post processing:

$$p_k \rightarrow p_k e^{-j2\pi f_{\text{bin}} \tau_{\text{residual}} k}, \quad (6)$$

where  $\tau_{\text{residual}}$  is the residual delay.

Note that above operations are mathematically identical, and the modulations are linear, which can be expressed as:

$$x_k \rightarrow x_k e^{j\alpha k}. \quad (7)$$

In classical signal processing, phase modulation for a sequence of length  $N$  is pointwise, which yields a computational complexity of  $O(N)$ . However, in the quantum computation framework, the linear phase modulation can be represented by the unitary operator:

$$P(\alpha) : |k\rangle \rightarrow e^{j\alpha k} |k\rangle. \quad (8)$$

The corresponding phase factor for  $n$  qubits can be written as:

$$e^{j\alpha k} = \prod_{i=0}^{n-1} e^{j\alpha 2^i k_i}, \quad (9)$$

which means the phase modulation can be implemented as a phase rotation gate  $P(\alpha 2^i)$  for the  $i$ -th qubit. Since quantum gates act globally on all components of a superposed quantum state, this operation modifies amplitudes of all  $N$  basis simultaneously. The computational complexity is reduced from  $O(N)$  of classic operations to  $O(n) = O(\log_2 N)$  of quantum operations.

## 2.3 Fourier transform

In VLBI data correlation, fringe-rotated baseband samples are Fourier transformed into the frequency domain for subsequent FSTC and cross-correlation. Classically, this step relies on the Fast Fourier Transform (FFT), which has a computational complexity of  $O(N \log_2 N)$ . In the quantum framework, an analogous operation is provided by the Quantum Fourier Transform (QFT). For an  $n$  qubit quantum state, the QFT acts on all  $2^n$  amplitude components simultaneously through a sequence of Hadamard gates and controlled-phase rotations, achieving an overall complexity of  $O(n^2)$ .

## 2.4 Cross correlation

We have to realize that quantum circuits are actually not suitable for direct output of full cross-power spectrum between two signals, since this involves the extraction of visibility in each individual frequency bin. The corresponding computational complexity is  $O(N)$ . Instead, when radio interferometric signals are encoded as quantum states of  $n$  qubits for each station, the cross correlation between the two stations is naturally the inner product of the corresponding quantum states.

Assuming  $|\psi_A\rangle$  and  $|\psi_B\rangle$  are Fourier transformed spectrum of station A and B, which can be expressed as

$$|\psi_A\rangle = \sum_{k=0}^{N-1} s_{a,k}|k\rangle, \quad |\psi_B\rangle = \sum_{k=0}^{N-1} s_{b,k}|k\rangle, \quad (10)$$

where  $s_{a,k}$  and  $s_{b,k}$  are the normalized complex spectrum at the  $k$ -th frequency point. The classical cross correlation, which is expressed as the sum of point-wise complex multiplications:

$$S = \sum_{k=0}^{N-1} s_{a,k}s_{b,k}^*, \quad (11)$$

is precisely the quantum mechanical inner product:

$$S = \mathcal{M}(\langle\psi_B|\psi_A\rangle) \quad (12)$$

Therefore, the cross correlation computation, or the coherent summation of cross spectrum across all frequency bins, is implicitly embedded into the multi-qubit Hilbert space and does not require evaluating each term  $s_{a,k}s_{b,k}^*$  individually. Note that the inner product is in quantum state and must be “read out” through a specific measurement  $\mathcal{M}$ . More specifically, in the quantum computing framework, this inner product can be extracted efficiently using Hadamard test. Let

$$U = U_B^\dagger U_A \quad (13)$$

be the composite operator such that:

$$U_A|0\dots0\rangle = |\psi_A\rangle, \quad U_B|0\dots0\rangle = |\psi_B\rangle, \quad (14)$$

then

$$\langle\psi_B|\psi_A\rangle = \langle 0\dots0|U|0\dots0\rangle. \quad (15)$$

The real and imaginary parts of above quantity can be obtained from single-qubit measurement statistics of the ancilla:

$$\text{Re}(\langle\psi_B|\psi_A\rangle) = 2 \text{Re}(P_0) - 1, \quad \text{Im}(\langle\psi_B|\psi_A\rangle) = 2 \text{Im}(P_0) - 1, \quad (16)$$

where  $\text{Re}(P_0)$  and  $\text{Im}(P_0)$  denote the probabilities of measuring the ancilla in state  $|0\rangle$  for the real and imaginary part of Hadamard tests, respectively.

As a result, the classical cross correlation operation, which requires a computational complexity of  $O(N)$ , is replaced by a single quantum inner-product extraction that acts on the entire  $2^n$ -dim superposition state.

Note that when the original baseband data is recorded using single side band (SSB), for  $N$  point real-sampled data, only the first  $N/2$  frequency bins are utilized after transforming to the frequency domain. Within the current quantum framework, this corresponds to extracting the coherently summed value

of the cross-power spectrum across the corresponding frequency bins. Since the cross-power spectrum is represented as a quantum superposition state within this framework, the first half of the spectrum corresponds to the subspace where the most significant qubit is in the  $|0\rangle$  state. As a result, a quantum circuit can be designed to apply a phase rotation operation to the  $(n - 1)$ -th qubit:

$$D(\theta) : |k_{n-1} \dots k_1 k_0\rangle \rightarrow e^{j\theta k_{n-1}} |k_{n-1} \dots k_1 k_0\rangle. \quad (17)$$

This operation can be incorporated into the composite operator defined in Eq. 13:

$$U(\theta) = U_B^\dagger D(\theta) U_A \quad (18)$$

Based on the binary representation of  $k$  in Eq. 3, the summed cross-power spectrum  $S$  as a function of  $\theta$  can be expressed as:

$$S(\theta) = \sum_{k=0}^{N/2-1} s_{a,k} s_{b,k}^* + \sum_{k=N/2}^{N-1} e^{j\theta} s_{a,k} s_{b,k}^* = S_0 + e^{j\theta} S_1. \quad (19)$$

The required component  $S_0$  can be obtained by performing measurements at  $\theta = 0$  and  $\theta = \pi$ :

$$S_0 = (S(0) + S(\pi))/2. \quad (20)$$

## 2.5 Fringe fitting

Fringe fitting is an important step in VLBI data post processing. As a first demonstration of applying quantum computation to VLBI data correlation, we consider a simplified scenario in which a single IF is used to estimate a single residual delay parameter  $\tau$ . The corresponding fitting function  $S(\tau)$  is given by:

$$S(\tau) = \sum_{k=0}^{N-1} s_{a,k} s_{b,k}^* e^{-j2\pi f_{\text{bin}} \tau k}. \quad (21)$$

The purpose of fringe fitting is to find out appropriate  $\tau$  that maximizes  $|S(\tau)|$ . In actual application, fringe fitting is a generalization of this simplified case, while the underlying principle remains the same.

For the quantum circuits in this work, the construction of the above fitting function corresponds to incorporating a linear phase modulation associated with the delay search into the composite operator defined in Eq. 13:

$$U(\tau) = U_B^\dagger P(2\pi f_{\text{bin}} \tau) U_A. \quad (22)$$

The summed value of the phase-modulated cross-power spectrum can be written as

$$\langle \psi_B | \psi_A \rangle(\tau) = \langle 0 \dots 0 | U(\tau) | 0 \dots 0 \rangle, \quad (23)$$

in its quantum state and then be extracted to obtain the fitting function:

$$S(\tau) = \mathcal{M}(\langle \psi_B | \psi_A \rangle(\tau)). \quad (24)$$

Fringe fitting can be regarded as a global optimization problem, in which the residual delay serves as the fitting parameter and the fitting function is the objective function. When the correct residual delay is identified, the fringe phase becomes flattened, and the objective function reaches its maximum. Within the present quantum algorithmic framework, the fitting function  $S(\tau)$  is evaluated for a series of trial delay  $\tau$  using the quantum procedure described above.

In our quantum algorithmic framework, the cross-correlation and fringe-fitting procedures are actually coupled together. In practice, one first determines a set of equally spaced trial delays based on the search range and step size. Then for each trial value  $\tau$ , the composite operator  $U(\tau)$  is constructed following the method described above, and the corresponding  $S(\tau)$  is obtained via Hadamard test. The residual delay is then identified as the value of  $\tau$  at which  $|S(\tau)|$  reaches its maximum.

It should be noted that, since  $\tau$  must be discretized in this procedure, there is a discrepancy between the discrete and the true maximum. Therefore, a further polynomial fit of the  $\tau \sim |S(\tau)|$  relation is usually required to further improve the estimation of the true maximum. This step is currently carried out classically and will be introduced in Sec. 3.1.4.

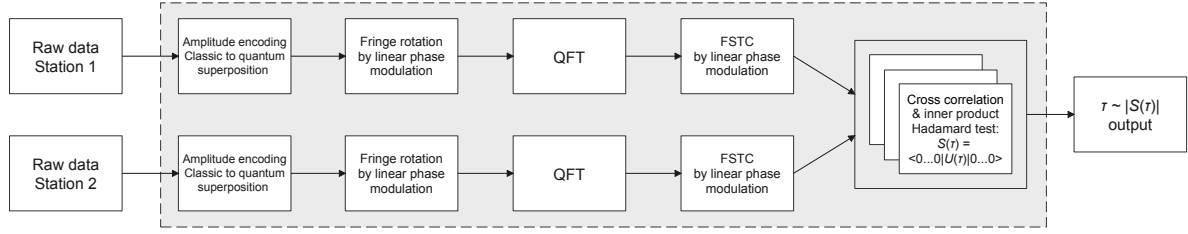


Figure 1: Dataflow of quantum pipeline. Quantum circuits are highlighted with gray background.

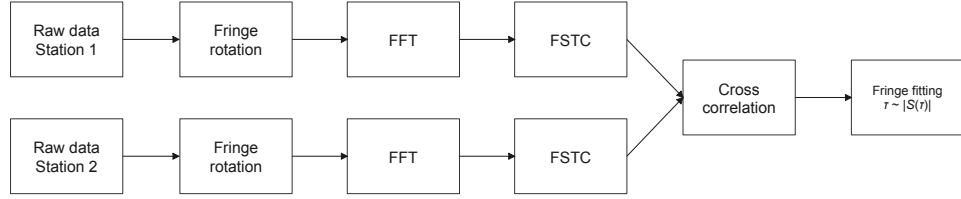


Figure 2: Dataflow of classical pipeline.

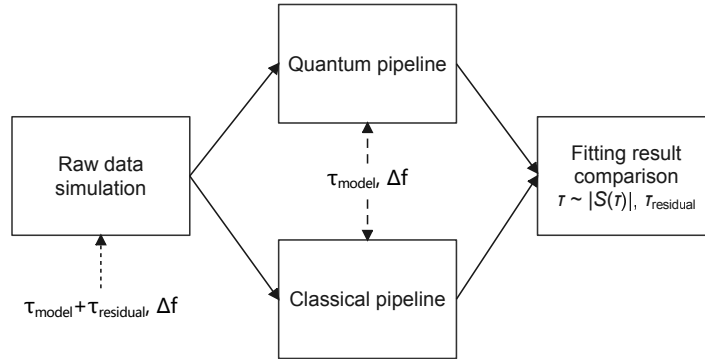


Figure 3: Architecture for the comparison between quantum and classical pipelines.

### 3 Demonstration of quantum processing pipeline

As the demonstration of above quantum based framework, in this section, we construct the complete quantum VLBI data correlation pipeline, perform correlation and fringe fitting with this pipeline, and compare the quantum derived delay estimation with those obtained from classical pipeline.

#### 3.1 Architecture of the system

To validate the quantum algorithm proposed in this work, in addition to the quantum pipeline itself, we also developed a raw-data simulation module for testing, a classical pipeline corresponding to the quantum algorithm, and a classical polynomial fitting module to achieve higher accuracy for residual delay fitting. The overall architecture is shown in Fig. 3.

##### 3.1.1 Raw data simulation

Two streams of baseband data are generated with given delay and fringe rate. Note that the input delay for generating raw data composes of two part: the model part  $\tau_{\text{model}}$ , which will be compensated in the quantum/classical pipeline, and the residual part  $\tau_{\text{residual}}$ , which will be used as reference value for the evaluation of the two pipelines' data correlation result.

##### 3.1.2 Quantum pipeline

The quantum pipeline is implemented with **Qiskit**. Classical raw data of length  $N$  are embedded into quantum system with  $n = \log_2 N$  qubits via amplitude encoding. The linear phase modulation operators for fringe rotation and FSTC are constructed based on Eq. 8. Besides that, this operator is also used in the construction of composite operator  $U(\tau)$ . The transform from time domain to frequency domain is performed with QFT. The inner-product of two quantum spectrum are extracted via Hadamard test. To support fringe fitting, for each trial residual delay  $\tau$ , the composite operator  $U(\tau)$  is constructed according to Eq. 22.

##### 3.1.3 Classical pipeline

In classical VLBI data correlation pipeline, the whole process can be divided into two stages. The first stage is cross correlation, including fringe rotation, FFT, FSTC and cross correlation. The cross spectrum is saved for further analysis. The second stage is post processing: for each tentative delay  $\tau$ ,  $S(\tau)$  is calculated according to Eq. 21. The differences between quantum and classical pipeline are clearly demonstrated in Fig. 1 and 2. In our current implementation, the fringe rotation, FSTC and delay compensation are implemented according to Eq. 4, 5 and 6. The Fourier transform is performed with standard FFT.

##### 3.1.4 Polynomial fit & comparison

In VLBI data post processing, polynomial fit for the discretized values of  $|S(\tau)|$  is usually performed, so as to achieve a better estimation of the residual delay. The procedure is:

- Identify the maximum amplitude and the corresponding delay from a series of equally spaced trial delays for the given search range and step size.
- Perform second order polynomial fit for the consecutive 5 points around the maximum amplitude, with  $x$  and  $y$  correspond to  $\tau$  and  $|S(\tau)|$ , respectively.
- Derive  $\tau$  ( $x$ ) that corresponds to the maximum value of the polynomial curve. If required, also derive the uncertainty of delay  $\sigma_\tau$  based on the covariance matrix.

The  $\tau \sim |S(\tau)|$  relations from both pipelines with identical raw data as input are fitted and compared, so as to evaluate the data correlation accuracy of the quantum pipeline. The raw cross-spectrum before fringe fitting is dumped and plotted in Fig. 4. The slope of the fringe phase corresponds to the pre-set residual delay. Since our simulated data are single side band (SSB), only the first half frequency bins are adopted. In the quantum pipeline, the summed cross spectrum of this part is extracted via Hadamard test as explained in Sec. 2.4.

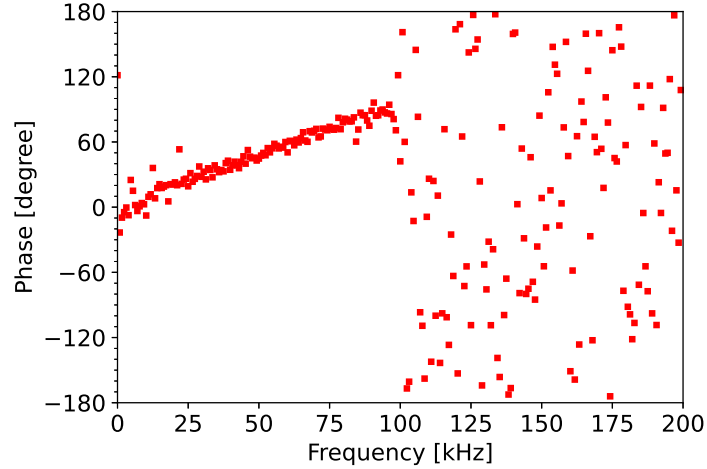


Figure 4: Demonstration of the cross spectrum after correlation. Red square represents phase value at the corresponding frequency bin. For single side band (SSB) data used for pipeline verification in this work, only the first half frequency bins contain useful information. Since delay compensation is not performed, the fringe is not flat. The fitting of the slope yields the residual delay listed in Tab. 1

Parameter	Value
Mode	Single side band (SSB)
Sampling number	256
Qubit number	8
Bandwidth	0.1 MHz
Input/model fringe rate ( $\Delta f$ )	500 Hz
Input delay ( $\tau_{\text{model}} + \tau_{\text{residual}}$ )	6.7 $\mu\text{s}$
Model delay ( $\tau_{\text{model}}$ )	4.0 $\mu\text{s}$
Residual delay ( $\tau_{\text{residual}}$ )	2.7 $\mu\text{s}$

Table 1: Simulation parameters for quantum pipeline verification.

### 3.2 Simulation setup & result

The parameters for quantum pipeline verification are listed in Tab. 1. The input fringe rate and delay are used for raw data generation. The model fringe rate and delay are adopted for frequency and delay correction in the correlation process. The residual delay is kept as the reference value for the verification of the two pipelines.

Fig. 5 demonstrates the  $\tau \sim |S(\tau)|$  relationships as the output of both classic and quantum pipelines. In general, the amplitudes of the two pipelines agree well with each other. Each pipelines derive a residual delay that is close to the real value. For polynomial fitting around the maximum amplitude, the quantum pipeline yields 12 times larger uncertainty. This could be attributed to the shooting noise when the quantum inner product is read out via Hadamard test. We have observed that the discrepancies between the quantum pipeline and the classical pipeline decrease as the number of shots increases. In the current work, the `shots` parameter is set to 20000.

## 4 Discussion

### 4.1 Amplitude encoding

In this work, amplitude encoding is adopted to load classical raw data into quantum superposition states. However, given the current capabilities of quantum circuits, preparing an arbitrary quantum state remains a major challenge even in the algorithm level. A computational complexity of  $O(N)$  for encoding  $N$  samples makes it the most expensive component of the entire quantum framework.

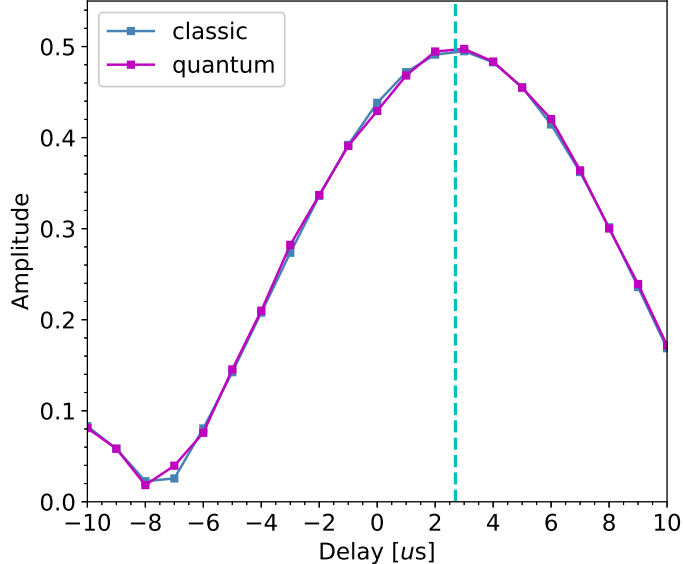


Figure 5: The amplitude of the summed cross-spectrum after delay compensation  $|S(\tau)|$  as a function of trial delay  $\tau$ . Blue and magenta lines correspond to the fitting result of classic and quantum pipelines, respectively. Cyan dashed line represents the input residual delay  $\tau_{\text{residual}} = 2.7 \mu\text{s}$ . The derived residual delay and uncertainty for classic and quantum pipelines are:  $2.734 \pm 0.003 \mu\text{s}$  and  $2.791 \pm 0.037 \mu\text{s}$ .

Actually data loading is widely recognized as the main bottleneck that of many quantum algorithms (Au-Yeung et al., 2024).

Notice that VLBI baseband data are always recorded in quantized form, e.g., in the 1-bit case, all samples have the same magnitude and differ only in sign, and large contiguous regions may contain identical values. By exploiting these patterns and employing a binary-tree structure, in the best case it is possible to reduce the complexity of loading  $N$  samples to  $\log_2 N$ . We plan to implement this amplitude-encoding scheme in future work and evaluate its performance using real VLBI raw baseband data.

## 4.2 Integration of cross spectrum

The quantum algorithm presented in this work demonstrates cross-correlation of only a single Fourier transform (FT) period. In practice, VLBI data correlation requires coherent accumulation of cross-power spectra over many FT periods so as to improve the signal-to-noise ratio. Notably, the Hadamard test described in Sec. 2.4 yields a coherently summed cross spectrum. Therefore, for each FT period, one may compute the corresponding fringe-rotation and FSTC term from the delay model, construct the composite operator  $U(\tau)$  for a series of trial delays, and measure  $S_n(\tau)$ , where  $n$  denotes the  $n$ -th FT period. Coherent summation along the time axis can then be performed to achieve the desired integration.

## 4.3 Fringe fitting

In the current framework, the quantum circuit is used to compute the fitting function  $S(\tau)$  for a set of uniformly distributed trial delays  $\tau$  within a given search range, after which a classical search is performed to identify the maximum amplitude. To improve the accuracy of the search, a smaller step size is desirable, which increases the computational cost. It is worth noting that the Durr–Hoyer algorithm, which is the extension of the classical Grover search (Grover, 1996), can locate the maximum of a function defined on a discretized grid with complexity reduced from  $O(N)$  to  $O(\sqrt{N})$  (Durr & Hoyer, 1996). However, the implementation of above approach requires several modifications to the current quantum algorithm.

First of all, the set of trial delay values must be loaded into quantum superposition state, which can be performed using the linear phase-modulation technique introduced in Sec. 2.2. Second, the cross-correlation computation must be encapsulated into an oracle, with the trial delay value provided as a kind of “argument” to the quantum circuit, rather than constructing a separate circuit for each  $\tau$  as done in the current design. Finally, since Grover-type algorithms require the oracle output to be coherent and reversible, the present Hadamard test based estimation cannot be used. A fully quantum-compatible method for amplitude evaluation or comparison must be developed instead. Most of these modifications are non-trivial and will require further investigation.

## 5 Conclusion

In this work, we demonstrate that VLBI data correlation is naturally compatible with quantum computation in several fundamental respects. On the one hand, a quantum state encoded in  $n$  qubits spans a  $2^n$ -dimensional Hilbert space, enabling the representation of large volumes of raw baseband data using only  $\log_2 N$  qubits. Such kind of quantum encoding provides a powerful form of data “compression” that is unachievable in classical systems. On the other hand, the basic operations in VLBI correlation and fringe fitting, including linear phase modulation, Fourier transform, and cross correlation, can be efficiently implemented via quantum circuits with lower computational complexity.

Based on these insights, we constructed a quantum VLBI data correlation pipeline using `Qiskit`, together with a corresponding classical pipeline for verification. Using simulated baseband data, we tested the full workflow, including fringe rotation, Fourier transform, FSTC, cross correlation, and fringe fitting. The comparison between classical and quantum results shows that the proposed quantum framework successfully reproduces the expected summed cross-spectrum and yields correct residual delay estimation, therefore validating both the correctness and feasibility of the quantum approach.

Despite these promising results, several challenges remain before quantum computing can be applied to actual VLBI data correlation, particularly regarding quantum state preparation. Loading classical data into quantum superposition state via amplitude encoding is one of the major bottlenecks for quantum algorithms broadly, not merely for VLBI applications. Notably, VLBI raw baseband samples are typically quantized to 1 or 2 bits and exhibit repeated patterns, both of which can be investigated to reduce loading complexity. These characteristics suggest the feasibility of efficient state-preparation schemes.

In general, this study demonstrates that quantum computing provides a promising framework for VLBI data correlation. With continued advances in quantum hardware, quantum-assisted algorithms may become a practical and powerful tool for next-generation VLBI projects.

The necessary data and code for the quantum pipeline will be available and updated in the GitHub repository: <https://github.com/liulei/qcorr>.

## References

Arute, F., Arya, K., Babbush, R., et al. 2019, *Nature*, 574, 7779, 505. doi:10.1038/s41586-019-1666-5

Au-Yeung, R., Camino, B., Rathore, O., et al. 2024, *Reports on Progress in Physics*, 87, 11, 116001. doi:10.1088/1361-6633/ad85f0

Deller, A. T., Brisken, W. F., Phillips, C. J., et al. 2011, *PASP*, 123, 901, 275. doi:10.1086/658907

Deutsch, D. 1985, *Proceedings of the Royal Society of London Series A*, 400, 1818, 97. doi:10.1098/rspa.1985.0070

Dewdney, P. E., Hall, P. J., Schilizzi, R. T., et al. 2009, *IEEE Proceedings*, 97, 8, 1482. doi:10.1109/JPROC.2009.2021005

Duev, D. A., Molera Calvés, G., Pogrebenko, S. V., et al. 2012, *A&A*, 541, A43

Durr, C. & Hoyer, P. 1996, *quant-ph/9607014*. doi:10.48550/arXiv.quant-ph/9607014

Event Horizon Telescope Collaboration, Akiyama, K., Alberdi, A., et al. 2019, *ApJL*, 875, L1

Feynman, R. P. 1982, *International Journal of Theoretical Physics*, 21, 6-7, 467. doi:10.1007/BF02650179

Gao, D., Fan, D., Zha, C., et al. 2025, *PRL*, 134, 9, 090601. doi:10.1103/PhysRevLett.134.090601

Grover, L. K. 1996, *quant-ph/9605043*. doi:10.48550/arXiv.quant-ph/9605043

Haas, R., Nothnagel, A., & Petrachenko, B. 2015, *IAU General Assembly*, 29, 2257511.

Javadi-Abhari, A., Treinish, M., Krsulich, K., et al. 2024, *arXiv:2405.08810*. doi:10.48550/arXiv.2405.08810

Kondo, T. & Takefuji, K. 2016, *Radio Science*, 51, 10, 1686. doi:10.1002/2016RS006070

Michael, A. & Chuang, I. L. 2010, *Quantum Computation and Quantum Information* (2nd ed.). Cambridge: Cambridge University Press

Shor, D. 1994, *Proc. 35th IEEE Symp. on Foundations of Computer Science*, Santa Fe, NM, USA, 124. doi: 10.1109/SFCS.1994.365700

Simon, D. R. 1994, *Proc. 35th IEEE Symp. on Foundations of Computer Science*, Santa Fe, NM, USA, 116. doi: 10.1109/SFCS.1994.365701

Thompson, A. R., Moran, J. M., & Swenson, G. W. 2017, *Interferometry and Synthesis in Radio Astronomy*, by A. Richard Thompson, James M. Moran, and George W. Swenson, Jr. 3rd ed. Springer, 2017.. doi:10.1007/978-3-319-44431-4

Whitney, A. R. 2007, *Proceedings of the 18th European VLBI for Geodesy and Astrometry Work Meeting*, 79, 33.

Zheng, W., Quan, Y., Shu, F., et al. 2010, *Sixth International VLBI Service for Geodesy and Astronomy. Proceedings from the 2010 General Meeting*, 157

Zhong, H.-S., Wang, H., Deng, Y.-H., et al. 2020, *Science*, 370, 6523, 1460. doi:10.1126/science.abe8770

Zhu, R., Wu, Y., & Li, J. 2016, *New Horizons with VGOS*, 163.